

# The Flavor Structure of the Excited Baryon Spectra from Lattice QCD

Robert G. Edwards,<sup>1,\*</sup> Nilmani Mathur,<sup>2,†</sup> David G. Richards,<sup>1,‡</sup> and Stephen J. Wallace<sup>3,§</sup>  
(for the Hadron Spectrum Collaboration)

<sup>1</sup>*Jefferson Laboratory, 12000 Jefferson Avenue, Newport News, VA 23606, USA*

<sup>2</sup>*Department of Theoretical Physics, Tata Institute of Fundamental Research, Homi Bhabha Road, Mumbai 400005, India*

<sup>3</sup>*Department of Physics, University of Maryland, College Park, MD 20742, USA*

(Dated: December 20, 2012)

Excited state spectra are calculated using lattice QCD for baryons that can be formed from  $u$ ,  $d$  and  $s$  quarks, namely the  $N$ ,  $\Delta$ ,  $\Lambda$ ,  $\Sigma$ ,  $\Xi$  and  $\Omega$  families of baryons. Baryonic operators are constructed from continuum operators that transform as irreducible representations of  $SU(3)_F$  symmetry for flavor,  $SU(4)$  symmetry for Dirac spins of quarks and  $O(3)$  symmetry for orbital angular momenta. Covariant derivatives are used to realize orbital angular momenta. Using the operators, we calculate matrices of correlation functions in order to extract excited states. The resulting lattice spectra have bands of baryonic states with well-defined total spins up to  $J = \frac{7}{2}$ . Each state can be assigned a dominant flavor symmetry and the counting of states of each flavor and spin reflects  $SU(6) \times O(3)$  symmetry for the lowest negative-parity and positive-parity bands. States with strong hybrid content are identified through the dominance of chromo-magnetic operators.

## I. INTRODUCTION

The spectra of baryon resonances have been a focus of study experimentally and theoretically, both for particles composed of the light  $u$  and  $d$  quarks, and those containing one or more of the heavy  $c$  and  $b$  quarks. There is increasing activity aimed at understanding the spectra of particles containing one or more  $s$  quarks, so-called hyperon physics, e.g., [1]. At present the knowledge of the  $\Xi$  and  $\Omega$  families is particularly limited with only a few states experimentally established, and scant knowledge as to their properties [2]. Two recent lattice studies have focused on the lowest few states of  $N$  [3] and  $\Lambda$  [4].

A quantitative description of the spectra of baryons that can be constructed from the  $u$ ,  $d$  and  $s$  quarks is important for a number of reasons. Firstly, to explore how the effective degrees of freedom that describe the hadron spectra change as the masses of the quarks are changed. Secondly, to advance our understanding of QCD in regimes where the hyperons play a crucial role, such as in the physics of the early universe and core-collapse in supernovae. Finally, to address the long-term goal of extracting baryon spectra from lattice QCD.

In this paper, we present lattice QCD calculations of the excited-state spectra of baryons that can be constructed from  $u$ ,  $d$  and  $s$  quarks: the  $N$ ,  $\Delta$ ,  $\Lambda$ ,  $\Sigma$ ,  $\Xi$  and  $\Omega$  families of baryons. Our calculations exploit a menu of methods that we have developed and are key to our studies of excited-state spectra: the use of an anisotropic, clover action for the generation of gauge configurations [5, 6], the construction of operators that respect the symmetries of the lattice yet which retain a

memory of their continuum analogues [7], the use of “distillation” [8] to efficiently compute the correlation functions between those operators, and finally the application of the variational method [9, 10], exploiting the eigenvectors of matrices of correlation functions to determine the spins and flavors of the extracted energies. In two earlier works, Refs. [7, 11], we applied these methods to compute the nucleon and  $\Delta$  spectra, with the spins of the states identified clearly; these works revealed spectra at least as rich as the quark model, with suggestions of “hybrid” states in which the gluons played an important structural role. Here we expand upon these works by considering baryons containing not only the light  $u$  and  $d$  quarks, but also one or more  $s$  quarks.

The layout of the remainder of the paper is as follows. In the next section, we describe details of the lattices used, and outline the construction of the lattice interpolating operators. In Sec. II B, we recall our procedure for analyzing the hadron correlation functions, and for identifying the continuum spins of the states. Our results are presented in Sec. III and a summary of the work is presented in Sec. IV.

## II. COMPUTATIONAL METHODS AND DETAILS

A significant challenge in determining the excited-state spectra is to obtain a sufficient number of energy levels in order to extract their patterns of energies, spins and flavors before statistical noise overcomes the signal. This requires accurately resolving the behavior of hadron correlation functions at short temporal separations. A computationally efficient calculation is obtained through the use of an anisotropic action, with a finer temporal lattice spacing than that used in the spatial directions, enabling correlation functions to be resolved over several time slices while preserving a sufficient spatial volume. The lattice action used in this work, as well

\*Electronic address: edwards@jlab.org

†Electronic address: nilmani@theory.tifr.res.in

‡Electronic address: dgr@jlab.org

§Electronic address: stevewal@umd.edu

$a_t m_\ell$	$a_t m_s$	$m_\pi$	$m_K/m_\pi$	$a_t m_\Omega$	$N_{\text{cfigs}}$	$N_{\text{tsrcs}}$	$N_{\text{vecs}}$
-0.0743	-0.0743	702	1.00	0.3593(7)	500	7	56
-0.0808	-0.0743	524	1.15	0.3200(7)	500	7	56
-0.0840	-0.0743	391	1.39	0.2951(22)	479	8	56

TABLE I: Parameters of the  $16^3 \times 128$  lattices and propagators used in this work. The pion mass in MeV, and the number of configurations are listed, as well as the number of time-sources and the number of distillation vectors  $N_{\text{vecs}}$ .

as the method used to tune the parameters of the action, can be found in Refs. [5, 6]. To summarize, we use improved gauge and fermion actions with two mass-degenerate light quarks of mass  $m_l$  and a strange quark of mass  $m_s$ . We employ  $16^3 \times 128$  lattices having spatial lattice spacing  $a_s \sim 0.123$  fm, and a renormalized anisotropy, the ratio of the spatial and temporal lattice spacings, of  $\xi \approx 3.5$ . The calculation is performed at three values of the light-quark masses, corresponding to pion masses of 391, 524 and 702 MeV. The 702 MeV pion mass corresponds to the  $SU(3)_F$  flavor-symmetric point. Some details of the lattices are summarized in Table I.

### A. Baryon Interpolating operators

The construction of the baryon interpolating operators is described in Ref. [7]. Our starting point is to construct a set of continuum baryon interpolating operators, which we express symbolically as,

$$\mathcal{O}^{JP} \sim \left( F_{\Sigma_F} \otimes (S^{P_S})_{\Sigma_S}^n \otimes D_{L, \Sigma_D}^{[d]} \right)^{JP}, \quad (1)$$

where the factors  $F, S$  and  $D$  describe the flavor, Dirac spin and derivative structure of the operators, respectively, and the subscripts,  $\Sigma_i$ , denote the corresponding symmetry representations with respect to permutations. The Dirac spin factor,  $(S^{P_S})_{\Sigma_S}^n$ , represents the combination of three Dirac-spinor quark fields with overall angular momentum  $S$  and parity  $P_S$ , with permutational symmetry  $\Sigma_S$ , while  $n$  labels different constructions. The spatial factor,  $D_{L, \Sigma_D}^{[d]}$ , is expressed in terms of gauge-covariant derivatives acting on the three quark fields, where  $[d]$  denotes the number of derivatives,  $\Sigma_D$  is the permutation symmetry, and the derivatives are combined so as to transform as angular momentum  $L$ . Finally, the factors are combined to yield an interpolator of definite spin and parity, which we label  $JP$ .

The construction of operators is guided by symmetry considerations. Based upon four-component Dirac-spinor quark fields combined with  $SU(3)$  flavor plus angular momentum, the symmetry of the full set of operators is  $SU(12) \times O(3)$ . An important subset of operators is based on non-relativistic quark spins, by which we mean operators based on the upper two components of Dirac-spinor quark fields. In this study, we realize angular momenta by including up to two covariant derivatives,  $d = 0, 1, 2$ ,

with maximum accessible values of orbital angular momentum,  $L$ , of 0, 1, and 2, respectively. Tables II and III show the patterns of quantum numbers of operators based on non-relativistic spins. Not listed are operator constructions based on the lower components of Dirac spinors (relativistic quark spins), although they outnumber the non-relativistic operators in the set used.

Three non-relativistic quark spins are mixed-symmetric for  $S = \frac{1}{2}$  and symmetric for  $S = \frac{3}{2}$ . Orbital angular momenta are mixed-symmetric for  $L = 1$  and symmetric, mixed-symmetric or antisymmetric for  $L = 2$ . The combination of flavor, spin, and space symmetries must be symmetric to yield an operator that is antisymmetric when color is included, in accord with the Pauli Principle. We list in the tables the spin-parity,  $JP$ , of the distinct combinations that are allowed. The classification of operators according to  $SU(3)_F$  flavor symmetry will be exploited as a means of identifying the dominant flavor structure of the states in the extracted spectrum.

The operators constructed from non-relativistic quark spinors have the spin, parity and flavor quantum numbers allowed by  $SU(6) \times O(3)$  symmetry. These quantum numbers occur in definite patterns that are indicated by the bold numbers in Tables II and III, i.e., there are  $N_1(J)$ ,  $N_8(J)$  and  $N_{10}(J)$  operators for  $SU(3)_F$  singlet, octet and decuplet symmetries, respectively, with total angular momentum  $J$ . If the states in the spectra were to correspond to broken  $SU(6) \times O(3)$  symmetry, then there would be patterns with the same numbers of states and the same quantum numbers. We will compare our spectra with the  $SU(6) \times O(3)$  patterns given in Tables II and III.

For  $d = 2$ , the mixed-symmetry combination  $D_{L=1, M}^{[2]}$  corresponds to the commutator of two covariant derivatives, producing a chromo-magnetic field, as explained in Ref. [11]. We call these hybrid operators because of their essential gluonic content. The hybrid operators based on non-relativistic quark spinors are listed in Table IV. The patterns of states expected to be created by such hybrid operators correspond to the numbers  $M_1(J)$ ,  $M_8(J)$  and  $M_{10}(J)$ .

The final step in the construction of the interpolating operators is the subduction to the irreducible representations (irreps) of the cubic group. See Ref. [7] for details. The number of operators used in each lattice irrep is the same for both positive and negative parities, which are denoted by the subscripts  $g$  and  $u$ , respectively, and the operators are classified according to the flavor irreps of  $SU(3)_F$ , as shown in Table V.

In order to reduce the complexity of the analysis, some relativistic operators are omitted. We include all non-relativistic operators based on the upper-component Dirac spinors. For example, for  $\Sigma$ , 68 operators in irrep  $H$  are used, with 37 having flavor octet symmetry and 31 having flavor decuplet symmetry. This set omits 22 relativistic operators but is sufficient to determine the spectrum. Because we omit some relativistic operators, and

$SU(3)_F$	S	L	$J^P$		
$\mathbf{8}_F$	$\frac{1}{2}$	1	$\frac{1}{2}^-$	$\frac{3}{2}^-$	
	$\frac{3}{2}$	1	$\frac{1}{2}^-$	$\frac{3}{2}^-$	$\frac{5}{2}^-$
$N_8(J)$			<b>2</b>	<b>2</b>	<b>1</b>
$\mathbf{10}_F$	$\frac{1}{2}$	1	$\frac{1}{2}^-$	$\frac{3}{2}^-$	
$N_{10}(J)$			<b>1</b>	<b>1</b>	<b>0</b>
$\mathbf{1}_F$	$\frac{1}{2}$	1	$\frac{1}{2}^-$	$\frac{3}{2}^-$	
$N_1(J)$			<b>1</b>	<b>1</b>	<b>0</b>

TABLE II: Allowed spin-parity patterns for one-derivative operators based on non-relativistic quark spinors ( $SU(6) \times O(3)$  symmetry). For each flavor, the quark spin S and orbital angular momentum L are listed followed by the allowed  $J^P$  values. The total number of operators is listed as  $N_8$  for flavor octets,  $N_{10}$  for flavor decuplets and  $N_1$  for flavor singlets.

we include the “hybrid” operators introduced in Ref. [11], the number of operators differs from Ref. [7].

The spectra for the baryons made from  $u$  and  $d$  quarks, i.e.,  $N$  and  $\Delta$ , have been explored in earlier works using the same ensembles and operator constructions we will employ here, firstly in a calculation of the spectra for both parities but with the “hybrid” operators excluded from the basis[7], and then of the positive-parity spectra using all operators, including the “hybrid” operators[11]. In this work we consider excited states of both parities for baryons that can be formed from  $u$ ,  $d$  and  $s$  quarks.

## B. Correlator Analysis

The variational method we use in our analysis involves the computation of a matrix of correlation functions,

$$C_{ij}^A(t \equiv t_f - t_i) = \langle 0 | \mathcal{O}_i(t_f) \mathcal{O}_j^\dagger(t_i) | 0 \rangle, \quad (2)$$

for operators  $i$  and  $j$  that lie in a given cubic irrep,  $\Lambda$ . With the large operator basis introduced above, it is essential to have an efficient computational method for computing the baryon correlation functions. We use *distillation* [8], which provides a smearing function whilst enabling the full matrix of correlators to be constructed for all the operators at both source and sink. Following our earlier work using these lattices, we employ  $N = 56$  eigenvectors of the gauge-covariant Laplacian when constructing the distillation operator, and compute correlation functions from  $N_{\text{srcs}}$  time sources, as listed in Table I.

Our fitting strategy follows exactly that outlined in Refs. [7] and [11]. In summary, we solve the generalized

$SU(3)_F$	S	L	$J^P$			
$\mathbf{8}_F$	$\frac{1}{2}$	0	$\frac{1}{2}^+$			
	$\frac{1}{2}$	0	$\frac{1}{2}^+$			
	$\frac{1}{2}$	1	$\frac{1}{2}^+$	$\frac{3}{2}^+$		
	$\frac{1}{2}$	2		$\frac{3}{2}^+$	$\frac{5}{2}^+$	
	$\frac{1}{2}$	2		$\frac{3}{2}^+$	$\frac{5}{2}^+$	
	$\frac{1}{2}$	2		$\frac{3}{2}^+$	$\frac{5}{2}^+$	
	$\frac{1}{2}$	0		$\frac{3}{2}^+$	$\frac{5}{2}^+$	
	$\frac{1}{2}$	2	$\frac{1}{2}^+$	$\frac{3}{2}^+$	$\frac{5}{2}^+$	$\frac{7}{2}^+$
	$\frac{1}{2}$	2		$\frac{3}{2}^+$	$\frac{5}{2}^+$	$\frac{7}{2}^+$
	$\frac{1}{2}$	2		$\frac{3}{2}^+$	$\frac{5}{2}^+$	$\frac{7}{2}^+$
$N_8(J)$			<b>4</b>	<b>5</b>	<b>3</b>	<b>1</b>
$\mathbf{10}_F$	$\frac{1}{2}$	0	$\frac{1}{2}^+$			
	$\frac{1}{2}$	2		$\frac{3}{2}^+$	$\frac{5}{2}^+$	
	$\frac{1}{2}$	0		$\frac{3}{2}^+$	$\frac{5}{2}^+$	
	$\frac{1}{2}$	2		$\frac{3}{2}^+$	$\frac{5}{2}^+$	
	$\frac{1}{2}$	2	$\frac{1}{2}^+$	$\frac{3}{2}^+$	$\frac{5}{2}^+$	$\frac{7}{2}^+$
	$\frac{1}{2}$	2		$\frac{3}{2}^+$	$\frac{5}{2}^+$	$\frac{7}{2}^+$
$N_{10}(J)$			<b>2</b>	<b>3</b>	<b>2</b>	<b>1</b>
$\mathbf{1}_F$	$\frac{1}{2}$	0	$\frac{1}{2}^+$			
	$\frac{1}{2}$	2		$\frac{3}{2}^+$	$\frac{5}{2}^+$	
	$\frac{1}{2}$	1	$\frac{1}{2}^+$	$\frac{3}{2}^+$	$\frac{5}{2}^+$	
	$\frac{1}{2}$	2		$\frac{3}{2}^+$	$\frac{5}{2}^+$	
$N_1(J)$			<b>2</b>	<b>2</b>	<b>2</b>	<b>0</b>

TABLE III: Allowed spin-parity patterns for two-derivative operators based on non-relativistic quark spinors ( $SU(6) \otimes O(3)$  symmetry). For  $\mathbf{8}_F$ , two distinct operators with different internal symmetries are allowed for  $L=0$  combined with  $S=\frac{1}{2}$  and for  $L=2$  combined with  $S=\frac{1}{2}$ . Hybrid operators are listed separately in Table IV. The total number of operators for each spin is listed as  $N_8$  for flavor octets,  $N_{10}$  for flavor decuplets and  $N_1$  for flavor singlets.

eigenvalue equation,

$$C(t)v_n(t, t_0) = \lambda_n(t, t_0)C(t_0)v_n(t, t_0), \quad (3)$$

and thereby obtain the masses from the principal correlators,  $\lambda_n(t, t_0)$ ,  $\mathbf{n} = 1 \dots \dim(C)$ , by fitting to,

$$\lambda_n(t, t_0) = (1 - A_n)e^{-m_n(t-t_0)} + A_n e^{-m'_n(t-t_0)}. \quad (4)$$

The corresponding eigenvectors,  $v_n(t, t_0)$ , are aligned with those at reference time slice,  $t = t_{\text{ref}}$ , and they provide information as to the optimal interpolating operator for the state  $\mathbf{n}$ , namely  $\sum_i v_n^i \mathcal{O}_i^\dagger$ . Figure 1 shows fits of principal correlators for the ground state and eight excited states in the  $\Sigma$  spectrum for irrep  $H_g$ , where each state is identified as having spin-parity  $J^P = \frac{3}{2}^+$ . These states will be discussed later when we show how their spins and flavors can be identified and when we show that they form part of a pattern of states within the  $\Sigma$  spectrum.

As in Ref. [7], we make extensive use of the operator “overlap factors”,  $Z_i^n \equiv \langle \mathbf{n} | \mathcal{O}_i^\dagger | 0 \rangle$  that occur in the spec-

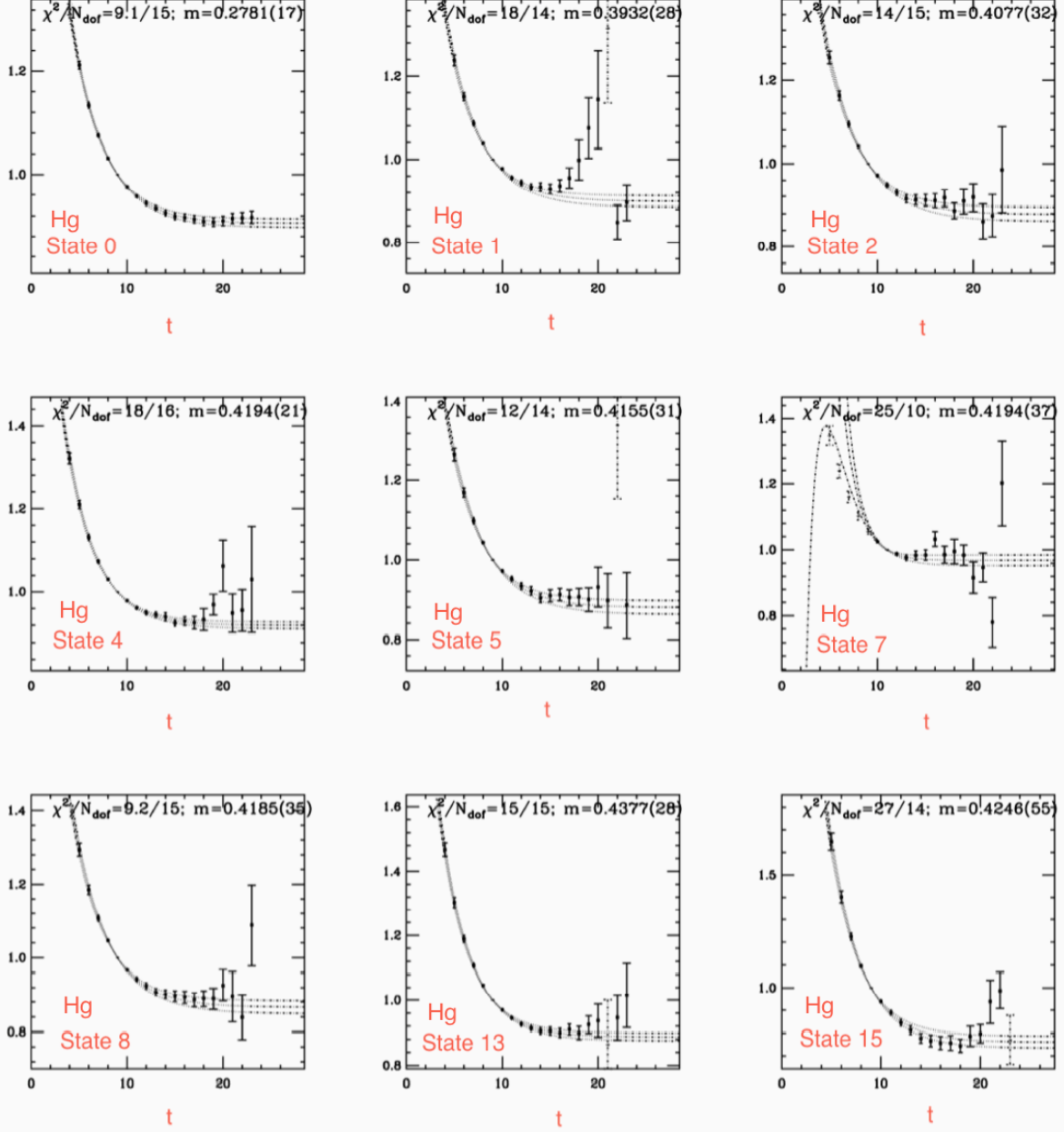


FIG. 1: Fits to principal correlators for nine states in irrep  $H_g$  that are identified as  $J = \frac{3}{2}^+$ . Fits are obtained using Eq. (4). For plotting, we divide out the first exponential factor, thus, the plots show values of  $e^{m_n(t-t_0)}\lambda_n(t)$  as the data points. Lines show the fits according to the form  $e^{m_n(t-t_0)}\lambda_n(t) = 1 - A_n + A_n e^{-(m'_n - m_n)(t-t_0)}$ , with  $t_0 = 9$ . The fits approach the constant value,  $1 - A_n$ , for large  $t$ . The bands indicate the fits with the central fit values along with one-standard-deviation uncertainties.

tral decomposition of the matrices of correlation functions,

$$C_{ij}(t) = \sum_n \frac{Z_i^{n*} Z_j^n}{2m_n} e^{-m_n t}. \quad (5)$$

Using the orthogonality condition for the eigenvectors

$v^{n\dagger} C(t_0) v^m = \delta_{n,m}$ , the overlap factors are related to the eigenvectors through  $Z_i^n = \sqrt{2m_n} e^{m_n t_0/2} v_j^{n*} C_{ji}(t_0)$ .

The baryon operators used in this work are constructed in two stages. The first stage is to construct operators in the continuum that have definite spin quantum numbers. In principle, these operators would produce a ma-

$SU(3)_F$	$S$	$L$	$J^P$		
$\mathbf{8}_F$	$\frac{1}{2}$ $\frac{3}{2}$ $\frac{3}{2}$	1  1	$\frac{1}{2}^+$ $\frac{1}{2}^+$ $\frac{3}{2}^+$	$\frac{3}{2}^+$ $\frac{3}{2}^+$ $\frac{5}{2}^+$	
$M_8(J)$			<b>2</b>	<b>2</b>	<b>1</b>
$\mathbf{10}_F$	$\frac{1}{2}$	1	$\frac{1}{2}^+$ $\frac{3}{2}^+$		
$M_{10}(J)$			<b>1</b>	<b>1</b>	<b>0</b>
$\mathbf{1}_F$	$\frac{1}{2}$	1	$\frac{1}{2}^+$ $\frac{3}{2}^+$		
$M_1(J)$			<b>1</b>	<b>1</b>	<b>0</b>

TABLE IV: Allowed spin-parity patterns for hybrid two-derivative operators based on non-relativistic quark spinors, following Ref. [11]. The operators correspond to the combination of three quarks in a color octet with a gluonic field,  $G$ , to make a color singlet as  $[(qqq)_{\mathbf{8}_c} G_{\mathbf{8}_c}]_{\mathbf{1}_c}$ . The gluon field has spin-parity  $1^+$ . The patterns of states expected to be created through the coupling of a chromo-magnetic gluon field coupled to quark fields in a color octet correspond to the numbers  $M_8$  for flavor octets,  $M_{10}$  for flavor decuplets and  $M_1$  for flavor singlets. The counting of operators is the same as in Table II but the operators have reversed parity.

	$SU(3)_F$	$I$	$S$	$G_1$	$H$	$G_2$
$N$	$\mathbf{8}_F$	$\frac{1}{2}$	0	22	37	15
$\Delta$	$\mathbf{10}_F$	$\frac{3}{2}$	0	19	31	12
$\Lambda$	$\mathbf{1}_F$	0	0	17	27	10
$\Lambda$	$\mathbf{8}_F$	0	0	22	37	15
$\Sigma$	$\mathbf{8}_F$	1	-1	22	37	15
$\Sigma$	$\mathbf{10}_F$	1	-1	19	31	12
$\Xi$	$\mathbf{8}_F$	$\frac{1}{2}$	-2	22	37	15
$\Xi$	$\mathbf{10}_F$	$\frac{1}{2}$	-2	19	31	12
$\Omega$	$\mathbf{10}_F$	0	-3	19	31	12

TABLE V: For each  $SU(3)_F$  symmetry, isospin  $I$  and strangeness  $S$ , the numbers of operators are shown in the last three columns for each lattice irrep  $G_1$ ,  $H$  and  $G_2$ . The constructions use operators with up to two derivatives. The same numbers of operators are used for both positive and negative parities.

trix of correlation functions that is orthogonal, i.e., proportional to  $\delta_{J,J'}$ , where  $J$  and  $J'$  are the spins of the source and sink operators. In the second stage of the construction, the operators are subduced to the irreps of the cubic group so that they can be used on a finite lattice. We observe that after the subduction, there remains a remarkable degree of rotational symmetry in the matrices of correlation functions that are obtained for baryons. They exhibit approximately the orthogonality property that holds in the continuum. An example of this is shown in Fig. 2, where the  $\Sigma$  correlator matrix,

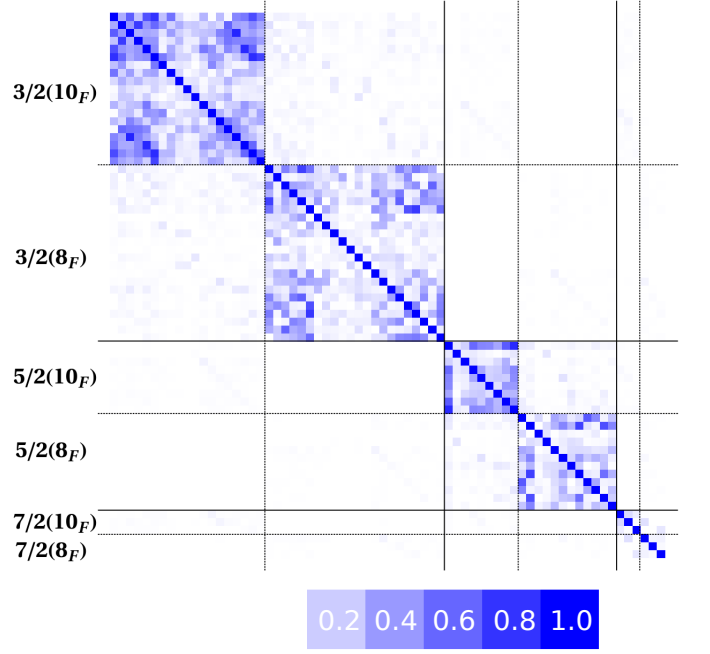


FIG. 2: Magnitudes of the elements of the correlator matrix,  $C_{ij}/\sqrt{C_{ii}C_{jj}}$ , at time-slice 5 are shown for  $\Sigma$  at  $m_\pi = 391$  MeV according to the darkness scale at the bottom. The blocks along the diagonal correspond to operators with the following spin-flavor combinations:  $\frac{3}{2}(\mathbf{10}_F)$ ,  $\frac{3}{2}(\mathbf{8}_F)$ ,  $\frac{5}{2}(\mathbf{10}_F)$ ,  $\frac{5}{2}(\mathbf{8}_F)$ ,  $\frac{7}{2}(\mathbf{10}_F)$  and  $\frac{7}{2}(\mathbf{8}_F)$ .

$C_{ij}(t)$ , is shown at  $t=5$  for irrep  $H_g$ , after normalizing each operator so that the diagonal elements are equal to one. The matrix indices range over 68 operators as follows: 19  $J = \frac{3}{2}$ ,  $\mathbf{10}_F$  operators; 22  $J = \frac{3}{2}$ ,  $\mathbf{8}_F$  operators; 9  $J = \frac{5}{2}$ ,  $\mathbf{10}_F$  operators; 12  $J = \frac{5}{2}$ ,  $\mathbf{8}_F$  operators; 3  $J = \frac{7}{2}$ ,  $\mathbf{10}_F$  operator; and 3  $J = \frac{7}{2}$ ,  $\mathbf{8}_F$  operators. The matrix is approximately block-diagonal with respect to  $J$ . Similar block-diagonal matrices of correlation functions are observed within other irreps and they stem from the construction of operators starting from definite continuum spins. These approximately orthogonal matrices are key to the identification of the continuum spin of states.

Although flavor symmetry remains a broken symmetry in the continuum because the strange quark in our calculations is heavier than the  $u$  and  $d$  quarks, the correlator matrix is approximately block diagonal with respect to flavor. As shown in Ref. [12], which uses the same lattices, the breaking of  $SU(3)_F$  symmetry is weak also for the mesons. When the operators of a given flavor symmetry are dominant, we exploit that feature to identify the dominant flavor composition of a state, and when hybrid operators play a substantial role we use that to identify states with strong hybrid content. Figure 3 illustrates how such identifications are made for states in the  $H_g$  irrep of the  $\Sigma$ . The plot shows the overlaps,  $Z_i^n$ , of

operators that create each state, with operators grouped by their continuum spin and flavor as indicated in the column labels at the top. The columns also are labeled by whether the operators are based on relativistic (R) or non-relativistic (NR) Dirac spinors, or hybrid constructions (h) or non-hybrid ones (nh). The operator overlaps provide a reasonable identification of the spin, flavor and hybrid content of the  $\Sigma$  states in irrep  $H_g$  of the cubic group. In particular, the identifications of states with spin-parity  $\frac{3}{2}^+$ , and flavor irreps  $\mathbf{8_F}$  or  $\mathbf{10_F}$ , are noted in the caption. Similar identifications are made to extract the patterns of other states in our spectra.

### III. RESULTS

In the following, we present the spectra in units of the  $\Omega$  mass determined on the corresponding ensemble. The spectra of  $N$ ,  $\Delta$ ,  $\Lambda$ ,  $\Sigma$ ,  $\Xi$  and  $\Omega$  families of baryons for spins up to  $\frac{7}{2}$  and both parities are shown at two different pion masses in Figures 4 and 5. The dominant flavor irrep is indicated by color: blue for  $\mathbf{8_F}$ , yellow for  $\mathbf{10_F}$ , and beige for  $\mathbf{1_F}$ . At the  $SU(3)_F$ -symmetric point, the spectra are shown in Fig. 6, now classified according to their  $SU(3)_F$  flavor irrep:  $\mathbf{8_F}$ ,  $\mathbf{10_F}$  or  $\mathbf{1_F}$ . Results for the positive parity  $N$  and  $\Delta$  spectra were presented earlier in ref. [11].

A general feature of the lattice spectra is that there are bands of excited states with alternating parities for each family of baryons: the lowest band of states for each parity is shown inside the slanted boxes. In the lowest negative-parity band, the numbers of states of each spin and flavor agree with the expectations shown in Table II, the table that shows the quantum numbers allowed by  $SU(6) \times O(3)$  symmetry for one-derivative operators.

In the lowest positive-parity band, the numbers of states for each spin and flavor agree with the expectations shown in Table III, the table that shows the quantum numbers allowed by  $SU(6) \times O(3)$  symmetry for two-derivative operators. While at the  $SU(3)_F$  symmetric point the counting involves a single flavor irrep, for the  $\Lambda$ ,  $\Sigma$  and  $\Xi$ , the correct numbers of states are obtained from summing the numbers for each of the two flavor irreps involved. This agreement between spectra and the expectations based on non-relativistic quark spins provides a clear signature of  $SU(6) \times O(3)$  symmetry in the spectra.

As noted in the caption of Fig. 3, the overlaps of the different operators classified according to their flavor structure provides a means of identifying the dominant flavor composition of the states in the spectra. Although the mixing of flavors increases as one moves away from the  $SU(3)_F$ -symmetric point, the dominant flavor identifications are shown by the different colors used in the plots of spectra. It is clear from our analysis that for the mixed-flavor states, the  $\Lambda$ ,  $\Sigma$  and  $\Xi$ , we find spectra that exhibit the multiplicities expected from exact  $SU(3)_F$  flavor symmetry for each of the flavor-identified

multiplets. In summary, the baryon spectra are remarkably consistent with the  $SU(6) \times O(3)$  expectations. It is this symmetry that is the basis for the quark model and the lowest bands of lattice states include the same quantum numbers that occur in the quark model [13–15].

In addition to the three-quark states that correspond to the quark model, a number of states are identified by their strong overlaps with hybrid interpolating operators, implying that they have a strong hybrid content. These states, in which the gluons play a substantive role, are shown for positive parity by symbols with thick borders in Figs. 4, 5 and 6. The two  $J = \frac{3}{2}^+$ ,  $\Sigma$  states in Fig. 4 with strong hybrid content and masses near  $1.6m_\Omega$  are  $H_g$  states 16 and 17 in Fig. 3. Note that the states with strong hybrid content generally are at high energy, typically about  $0.7m_\Omega$ , or more, above the ground state.

In this work we have no three-derivative operators. Because of that, and because the relativistic operators generally play an important role at higher energies, it is not meaningful to interpret the observed states at higher energies in terms of  $SU(6) \otimes O(3)$  symmetry. However, one sees qualitative similarity of the higher bands in Figs. 4 and 5 to the corresponding bands found at the flavor-symmetric point in Fig. 6.

It also is not meaningful to identify states with strong hybrid content in our negative-parity spectra and none are shown. Signals for states with significant hybrid content exist in negative-parity states at high energy, but they are based on the relativistic operators, whereas the three-derivative, non-relativistic operators that are absent may be equally, or more, important. Without a clear understanding of the relative importance of all the relevant operators, we cannot identify negative-parity states with strong hybrid content.

The baryon spectrum does not admit the “spin-parity exotics” that provide a useful indication of hybrid states in the meson spectrum, and indeed we observe that hybrid operators can have a significant, albeit not dominant, contribution to many states. Some examples can be found in Fig. 3, notably the lowest-lying spin- $\frac{3}{2}$  decuplet.

The patterns and multiplicities of positive-parity states with strong hybrid content can be compared with the expectations based on non-relativistic quark spins that are listed in Table IV. At the flavor symmetric point with  $m_\pi = 702$  MeV, which is shown in Fig. 6, and at  $m_\pi = 524$  MeV, which is shown in Fig. 5, one sees all the positive-parity hybrid states corresponding to Table IV. At  $m_\pi = 391$  MeV, which is shown in Fig. 4, most of the hybrid states are seen. One decuplet,  $J = \frac{1}{2}^+$  hybrid state is missing for  $\Sigma$ . An octet,  $J = \frac{3}{2}^+$  state and a decuplet,  $J = \frac{3}{2}^+$  state are missing for  $\Xi$ . These baryons involve mixings of  $\mathbf{8_F}$  and  $\mathbf{10_F}$  flavor symmetries and their spectra are particularly dense when subduced to the lattice irreps. For example, an  $H_g$  state must be found for each  $J = \frac{3}{2}$ ,  $\frac{5}{2}$  and  $\frac{7}{2}$  state in the spectrum. The  $\Xi$ ,  $J = \frac{5}{2}$  state with strong hybrid content was found as the

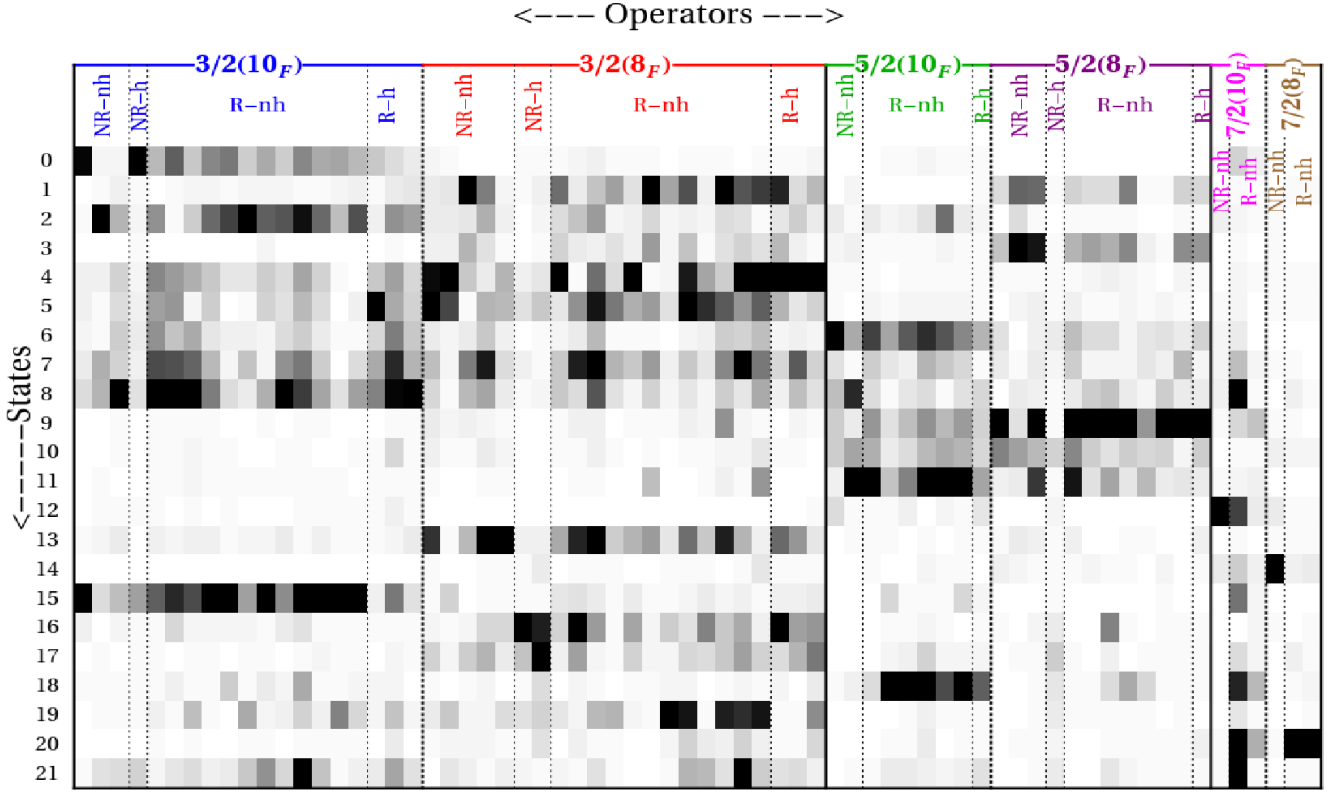


FIG. 3: “Matrix” plot of values of operator overlaps,  $Z_i^n$ , for state  $n$  and operator  $i$ , normalized according to  $\frac{Z_i^n}{\max_n [Z_i^n]}$  so that the largest overlap across all states for a given operator is unity. For each of the  $n = 0$  to 21 states of  $\Sigma$  in the  $H_g$  irrep, the magnitude of each operator’s overlap is shown for  $m_\pi = 391$  MeV. Darker pixels indicate larger values of the operator overlaps as in Fig. 2. Column labels indicate non-relativistic (NR) and relativistic (R) operators, as well as hybrid (h) and non-hybrid (nh) operators. In addition the flavor irrep is indicated as  $(10_F)$  for decuplet or  $(8_F)$  for octet and continuum spins of the operators are shown by  $\frac{3}{2}$ ,  $\frac{5}{2}$  and  $\frac{7}{2}$ . State 0, the ground state, and excited states 2, 8 and 15 are identified as  $J^P = \frac{3}{2}^+$  states with dominant decuplet flavor symmetry. States 1, 4, 5, 7 and 13 are identified as  $J^P = \frac{3}{2}^+$ , excited states with dominant octet symmetry. States 16 and 17 are  $J^P = \frac{3}{2}^+$  excited states with strong hybrid content and dominant octet flavor symmetry.

$29^{th}$  state in the  $H_g$  spectrum and was the highest state determined. The fact that a few of the states observed at higher values of the pion mass are not found at our lowest value of  $m_\pi$  may be because not all states have been determined. Overall, the lowest states with strong hybrid content are in reasonable accord with the expectations based on Table IV.

The excited states in the lowest bands of negative-parity are particularly well determined: Fig. 7 shows the ones that are created predominantly by flavor-octet operators and Fig. 8 shows the ones that are created predominantly by flavor decuplet and singlet operators. Note that we show the data for the mass of state  $n$ , namely  $m_n$ , in physical units that are obtained from the formula,  $m_n = 1672.45 \frac{m_{n,latt}}{m_{\Omega,latt}}$ , where  $m_{\Omega,latt}$  is the  $\Omega$  mass on the ensemble. Thus, the physical  $\Omega$  mass is used to set the scale. The patterns of these states are very similar for the different baryons. For the flavor-octet states, there are two  $\frac{1}{2}^-$  states, two  $\frac{3}{2}^-$  states and one  $\frac{5}{2}^-$  state. For each baryon, the energy increases with spin  $J$  and the

highest energy is about 300 MeV above the lowest energy, independent of the baryon. For the flavor decuplet case, there is one  $\frac{1}{2}^-$  state and one  $\frac{3}{2}^-$  state with about 70 to 100 MeV splitting,  $\Sigma_{10}$  being an exception. The flavor singlet case has the same pattern except that the energies are lower and the splitting is larger.

We note that there are several important limitations of the present study. They have been discussed in Ref. [7] and we conclude with a brief summary of them. The  $16^3 \times 128$  lattice used is small, with spatial dimensions of about 1.9 fm on a side. The pion masses used are significantly larger than the physical mass. No operators that efficiently couple onto scattering states (e.g.,  $\pi N$ ) are included. Studies of the resonances that correspond to the three-quark states will require improvements that overcome each of these limitations.

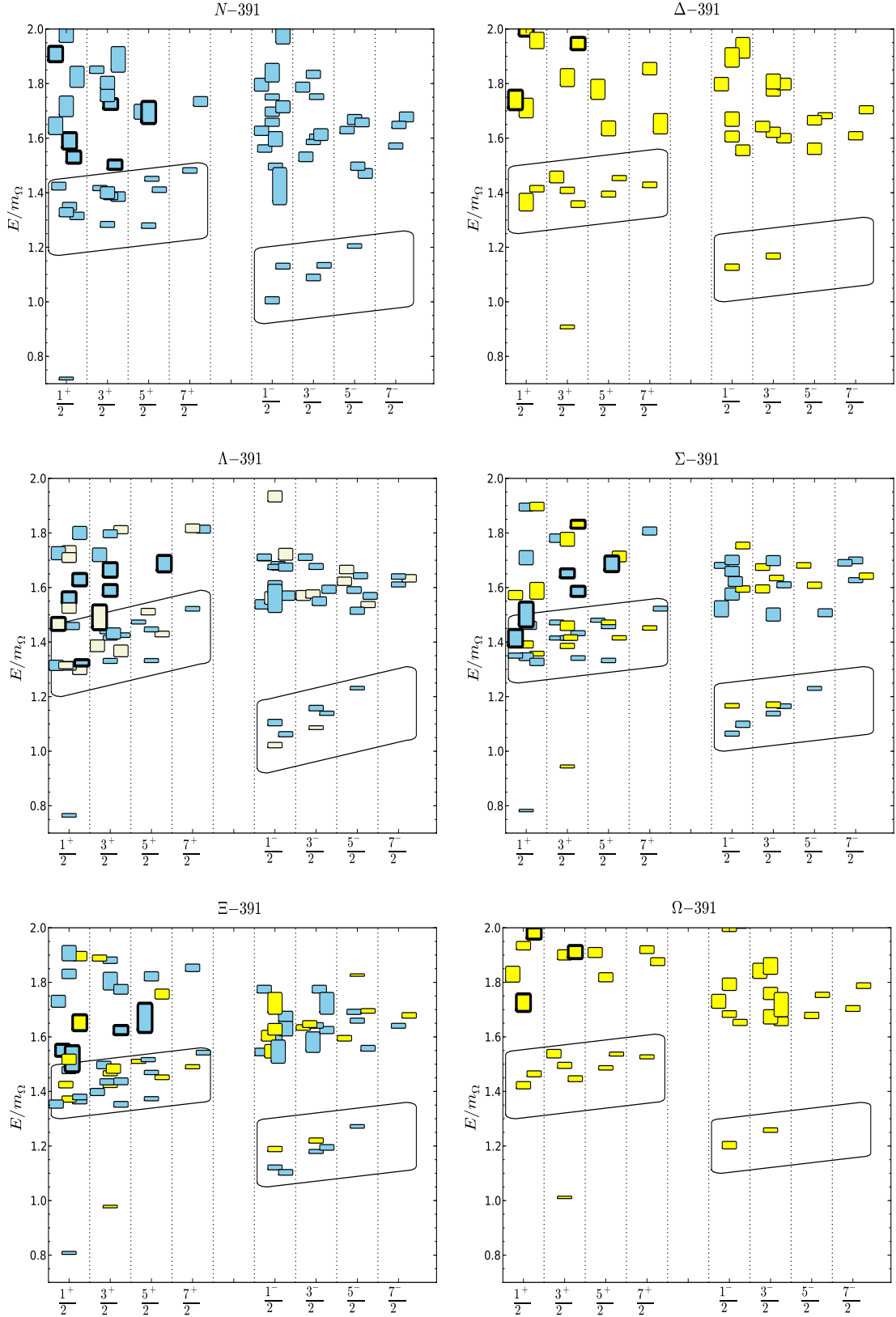


FIG. 4: Results for baryon excited states using the ensemble with  $m_\pi = 391$  MeV are shown versus  $J^P$ . Colors are used to display the flavor symmetry of dominant operators as follows: blue for  $8_F$ ; beige for  $1_F$ ; yellow for  $10_F$ . Symbols with thick border lines indicate states with strong hybrid content. Calculations are for a  $16^3 \times 128$  lattice. The lowest bands of positive- and negative-parity states are highlighted within slanted boxes. The eight excited states of  $\Sigma$ , with  $J^P = \frac{3}{2}^+$ , that are shown within a slanted box, are  $H_g$  states 1, 2, 4, 5, 7, 8, 13 and 15. Fits for the same states are shown in Fig. 1 and identifications of their spins and flavors are noted in Fig. 3.



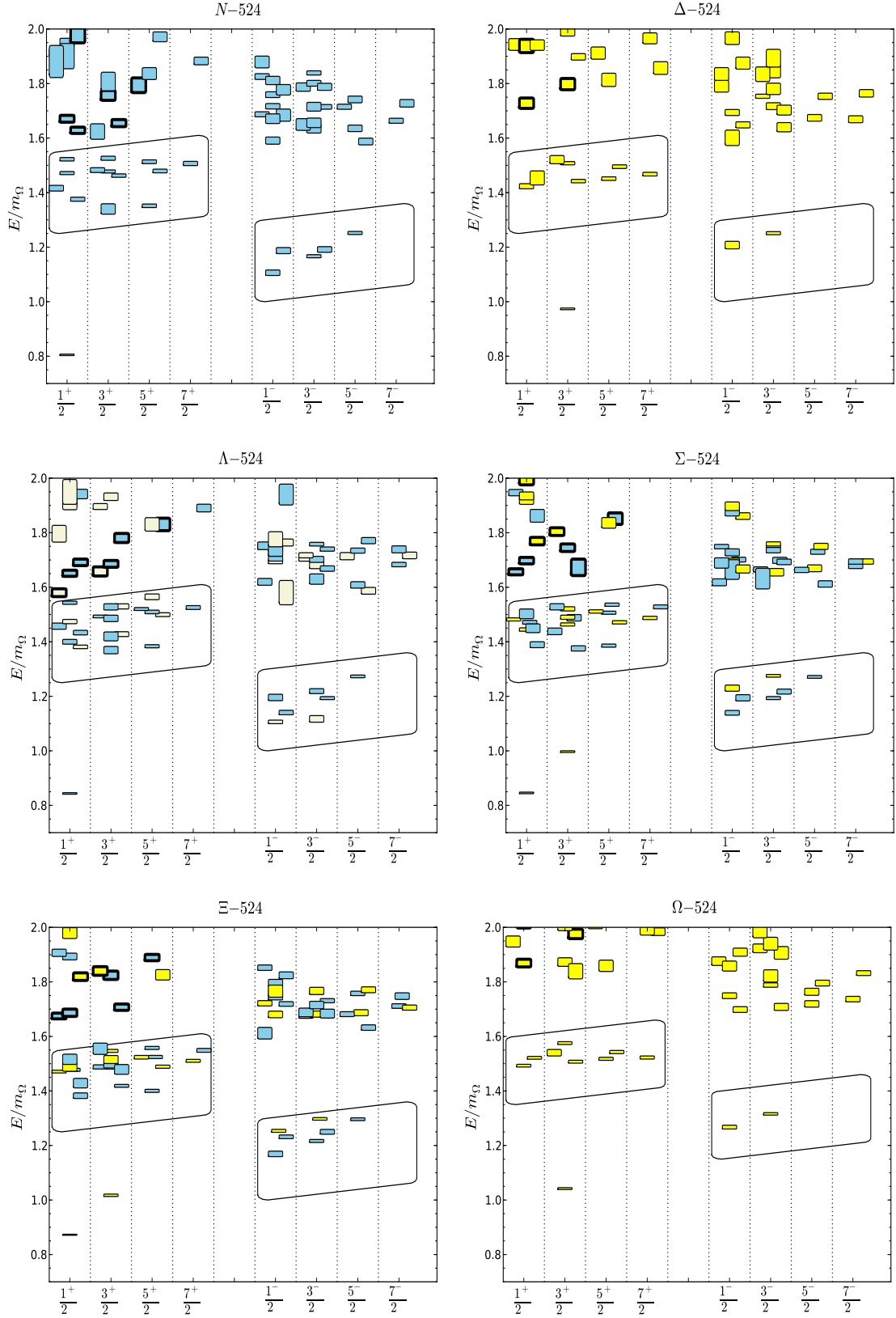


FIG. 5: Results for baryon excited states using the ensemble with  $m_\pi = 524$  MeV are shown versus  $J^P$ . Symbols are as described in Fig. 4.

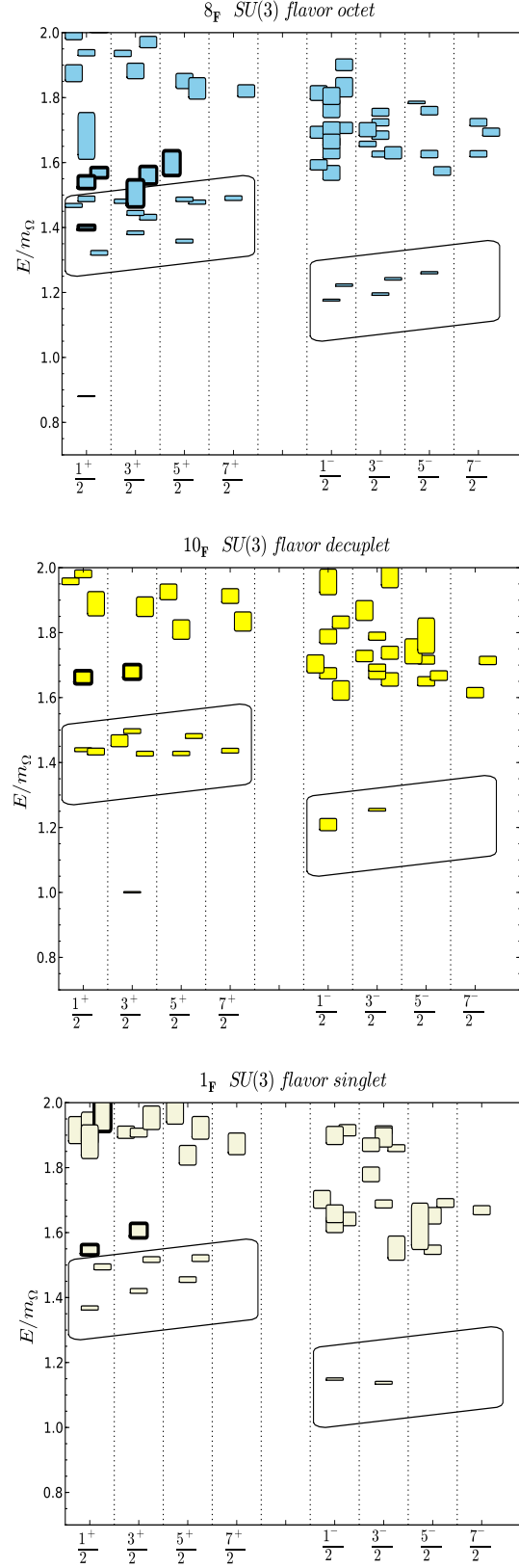


FIG. 6: Results for baryon excited states in flavor irreps  $8_F$ ,  $10_F$  and  $1_F$  obtained using the flavor-symmetric point, with  $m_\pi = 702$  MeV, are shown versus  $J^P$ . Symbols are as described in Fig. 4.

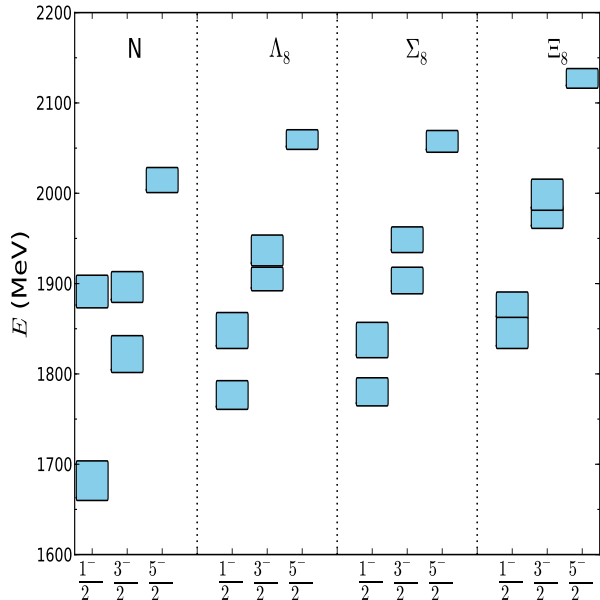


FIG. 7: The lowest negative-parity states that are flavor-octet are shown for  $m_\pi = 391$  MeV.

#### IV. SUMMARY

This work presents results for baryons based on lattice QCD using the  $16^3 \times 128$  anisotropic lattices that were developed in Ref. [6]. Excited state spectra are calculated for baryons that can be formed from  $u$ ,  $d$  and  $s$  quarks, namely the  $N$ ,  $\Delta$ ,  $\Lambda$ ,  $\Sigma$ ,  $\Xi$  and  $\Omega$  families of baryons, for two pion masses, 391 MeV, 524 MeV, and at the  $SU(3)_F$ -symmetric point corresponding to a pion mass of 702 MeV.

The interpolating operators used incorporate covariant derivatives in combinations that correspond to angular-momentum quantum numbers  $L = 0, 1$  and  $2$ . The angular momenta are combined with quark spins to build operators that transform according to good total angular momentum,  $J$ , in the continuum. As noted in earlier works, approximate rotational symmetry is realized at the scale of hadrons, enabling us to identify reliably the spins in the spectrum up to  $J = \frac{7}{2}$  from calculations at a single lattice spacing.

The operators we have employed are classified according to the irreducible representations of  $SU(3)_F$  flavor. At the pion masses used, the  $SU(3)_F$  symmetry is broken only weakly and states in the spectra can be identified as being created predominantly by operators of definite flavor symmetry  $\mathbf{8}_F$ ,  $\mathbf{10}_F$  or  $\mathbf{1}_F$ .

We find bands of states with alternating parities and increasing energies. Each state has a well-defined spin and generally a dominant flavor content can be identified. The number of non-hybrid states of each spin and flavor in the lowest-energy bands is in agreement with the

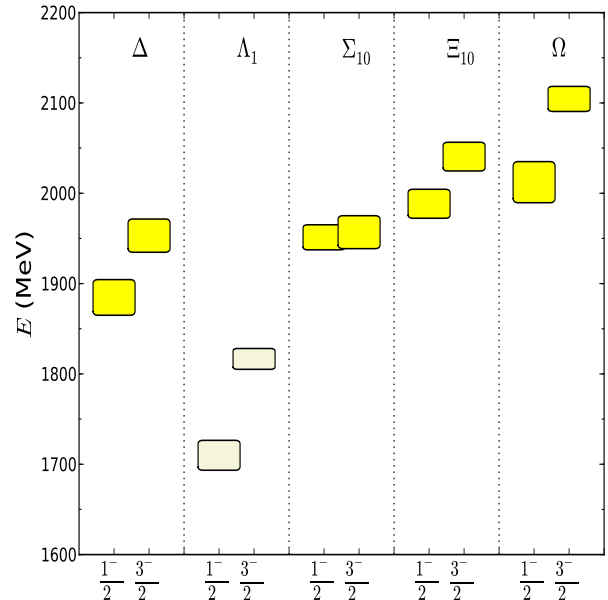


FIG. 8: The lowest negative-parity states that are flavor-singlet (beige) and decuplet (yellow) are shown for  $m_\pi = 391$  MeV.

expectations based on weakly broken  $SU(6) \otimes O(3)$  symmetry. These states correspond to the quantum numbers of the quark model.

Chromo-magnetic operators are used to identify states that have strong hybrid content. Usually these states are at higher masses, about  $0.7m_\Omega$ , or more, above the lowest non-hybrid states. There is reasonable agreement between the number of positive-parity states with strong hybrid content and the expectations of Table IV that are based on non-relativistic quark spins, although a few of the expected states are not found at the lowest pion mass.

With the inclusion into our basis of multi-hadron operators, which couple efficiently onto multi-hadron scattering states, we expect to find an increased number of levels in the spectrum. As demonstrated in Ref. [16], using the technique of moving frames where the total momentum of the system is nonzero, the increased number of levels allows for the extensive mapping of the energy dependence of scattering amplitudes, and hence, the determination of resonances. The prospect of determining the properties of resonances provides a strong motivation for continued work on the spectra of baryons.

#### Acknowledgments

We thank our colleagues within the Hadron Spectrum Collaboration. Particular thanks to C. Shultz for his updates to our variational fitting code. **Chroma** [17] and **QUDA** [18, 19] were used to perform this work on clusters

at Jefferson Laboratory under the USQCD Initiative and the LQCD ARRA project. Gauge configurations were generated using resources awarded from the U.S. Department of Energy INCITE program at Oak Ridge National Lab, the NSF Teragrid at the Texas Advanced Computer Center and the Pittsburgh Supercomputer Center, as well as at Jefferson Lab. SJW acknowledges support from

U.S. Department of Energy contract DE-FG02-93ER-40762. RGE, and DGR acknowledge support from U.S. Department of Energy contract DE-AC05-06OR23177, under which Jefferson Science Associates, LLC, manages and operates Jefferson Laboratory. NM acknowledges support from Department of Science and Technology, India, under grant No. DST-SR/S2/RJN-19/2007.

- 
- [1] B. Aubert et al. (BABAR Collaboration), *Phys.Rev.Lett.* **97**, 112001 (2006), hep-ex/0606039.
  - [2] J. Beringer et al. (Particle Data Group), *Phys.Rev.* **D86**, 010001 (2012).
  - [3] M. S. Mahbub, W. Kamleh, D. B. Leinweber, P. J. Moran, and A. G. Williams (CSSM Lattice Collaboration) (2012), 1209.0240.
  - [4] G. P. Engel, C. Lang, and A. Schafer (2012), 1212.2032.
  - [5] R. G. Edwards, B. Joo, and H.-W. Lin, *Phys. Rev.* **D78**, 054501 (2008), arXiv:0803.3960.
  - [6] H.-W. Lin et al. (Hadron Spectrum), *Phys. Rev.* **D79**, 034502 (2009), arXiv:0810.3588.
  - [7] R. G. Edwards, J. J. Dudek, D. G. Richards, and S. J. Wallace, *Phys.Rev.* **D84**, 074508 (2011), 1104.5152.
  - [8] M. Peardon et al. (Hadron Spectrum), *Phys. Rev.* **D80**, 054506 (2009), 0905.2160.
  - [9] C. Michael, *Nucl. Phys.* **B259**, 58 (1985).
  - [10] M. Luscher and U. Wolff, *Nucl. Phys.* **B339**, 222 (1990).
  - [11] J. J. Dudek and R. G. Edwards, *Phys.Rev.* **D85**, 054016 (2012), 1201.2349.
  - [12] J. J. Dudek et al., *Phys. Rev.* **D82**, 034508 (2010), 1004.4930.
  - [13] O. W. Greenberg, *Phys. Rev. Lett.* **13**, 598 (1964).
  - [14] N. Isgur and G. Karl, *Phys. Lett.* **B72**, 109 (1977).
  - [15] N. Isgur and G. Karl, *Phys. Rev.* **D18**, 4187 (1978).
  - [16] J. J. Dudek, R. G. Edwards, and C. E. Thomas (2012), 1212.0830.
  - [17] R. G. Edwards and B. Joo, *Nucl. Phys. B. Proc. Suppl.* **140**, 832 (2005).
  - [18] M. A. Clark et al., *Comput. Phys. Commun.* **181**, 1517 (2010), 0911.3191.
  - [19] R. Babich, M. A. Clark, and B. Joo, *ACM/IEEE Int. Conf. High Performance Computing, Networking, Storage and Analysis*, New Orleans (2010), 1011.0024.